

Electron Bernstein Wave Emission from an Overdense Plasma at the W7-AS Stellarator

H. P. Laqua, H. J. Hartfuß, and W7-AS Team

Max-Planck-Institut für Plasmaphysik, EURATOM Association,
D-85748 Garching, Germany
(Received 6 March 1998)

Thermal electron Bernstein wave (EBW) radiation of an overdense plasma ($n_e > n_{e,\text{cutoff}}$) was measured with an oblique viewing angle at the W7-AS stellarator. The spectrum consists of a local cyclotron-emission part and a nonlocal high-frequency part. Edge-temperature perturbations excited by carbon injection were used to demonstrate the relation between frequency and position of emission. Since for EBW's no density limit exists, the operation window of the electron-cyclotron-emission diagnostic can be extended to densities above the cutoff density. [S0031-9007(98)07009-4]

PACS numbers: 52.35.Hr, 52.25.Sw, 52.55.Hc

The accessible plasma density for electromagnetic electron-cyclotron waves is limited by the plasma cutoff. For the electrostatic electron Bernstein wave (EBW), the third electron-cyclotron mode which is able to propagate in a hot plasma, no such limit exists. However, since EBW's cannot leave the plasma directly, they have to be converted into electromagnetic waves first. This can be performed by the inverse process of O - X - B conversion, B - X - O , which was proposed by Preinhaelter and Kopecký for electron-cyclotron resonance heating (ECRH) [1] and which was recently demonstrated for fusion plasma heating in [2]. Here O , X , and B represent the ordinary, extraordinary, and the electron Bernstein modes. In the first step an O wave is converted into a slow X wave at the O -wave cutoff layer. In a second-mode conversion step an EBW is generated from the slow X wave at the upper hybrid resonance (UHR), where the X -mode branch of the solution of the hot plasma dispersion relation is connected to the electron Bernstein branch. For EBW's no density limit exists; they propagate towards the dense plasma center, where they are absorbed by cyclotron damping. Both mode conversions are reversible; thus the B - X - O process can also take place. The mode conversion process requires an optimal parallel component N_{\parallel} of the refractive index vector or, equivalently, an oblique detection near an optimal angle φ , a plasma density above the O -wave cutoff, and a frequency above the first cyclotron harmonic in the plasma. Since at the cyclotron resonance the plasma is optically thick for the EBW's, it is a blackbody emitter for EBW's, the same as it is for electromagnetic electron cyclotron waves below the cutoff density. But, in contrast to the electromagnetic waves for the EBW's, it is generally not possible to leave the plasmas since they have a density threshold for propagation at the upper hybrid resonance, which totally encloses the inner part of the plasma. Indeed, at the UHR, they can be converted into slow X waves, but these are also not able to leave the plasma and are backconverted to EBW's at their next contact with the UHR surface. The EBW radiation is trapped inside the plasma as in a hohlraum, ex-

cept for those EBW's which were born with an optimal N_{\parallel} (parallel to the magnetic field) for the B - X - O process or for those EBW's which had achieved such an N_{\parallel} component on their way in the plasma by scattering or magnetic configuration effects such as the field line curvature. The optimal N_{\parallel} or the optimal viewing angle φ , respectively, are defined by the following relation [1]: $N_{\parallel,\text{opt}}^2 = \cos^2(\varphi) = [Y/(Y + 1)]$ with $Y = \omega_{ce}/\omega$ (ω is the wave frequency and ω_{ce} is the electron cyclotron frequency). In a three-dimensional plasma, one also has to take into account the perpendicular (poloidal) refractive index N_{\perp} or the poloidal angle θ , but in our experiments no variation of N_{\perp} was performed. The shape of the angular window or the transmission function $T(N_{\perp}, N_{\parallel})$ depends on the density scale length $L = n_e/(\partial n_e/\partial x)$ and is given by Mjølhus [3] with

$$T(N_{\perp}, N_{\parallel}) = \exp\{-\pi k_0 L \sqrt{Y/2} \\ \times [2(1 + Y)(N_{\parallel,\text{opt}} - N_{\parallel})^2 + N_{\perp}^2]\},$$

where k_0 is the wave number. This angular dependence (N_{\parallel} dependence) of the emission was used in the experiments to identify electron Bernstein wave emission (EBE). Another criteria for EBE is the density threshold of the O - X - B and B - X - O processes, respectively. It takes place only if the density is above the O -mode cutoff density of the emitted frequency.

Ray tracing.—In model calculations with a ray tracing code for EBW's the emission and propagation of EBW's were simulated. We used the nonrelativistic hot dielectric tensor and an isotropic electron temperature. Since the full stellarator field geometry was not implemented in this code, the magnetic field configuration at the EBW propagation volume was approximated by a toroidally symmetric field with $B(r_{\text{eff}}) = B_0 A/(A + r_{\text{eff}}/a)$ ($A = 10.5$, $a = 0.1$ m) and no poloidal field was taken into account, which is sufficient to illustrate the basic features of the O - X - B -mode conversion and EBW propagation, but could not reproduce the experimental results completely. Especially, the measured Doppler shift of the EBW absorption

and emission differs from the ray-tracing calculation by about 4 GHz. This may originate from the simplification made in describing stellarator configuration.

Density and temperature profiles similar to typical neutral beam sustained W7-AS plasmas were used for these calculations. Since all processes of mode conversion and cyclotron emission are reversible, for simplicity the simulation was started at the detector. The ray trajectories were followed until 99% of the power was absorbed in the resonant case with cyclotron absorption inside the plasma. In the nonresonant case the calculation was stopped when the toroidal beam position exceeded the validity region of the approximated magnetic configuration ($\pm 3^\circ$ toroidal angle from the launch position). The ray trajectories for different frequencies are shown in Fig. 1. The shaded area indicates the plasma volume, where $1 - 1/e$ of the radiation is emitted, and shows the localization of resonant EBE. Each emitting volume is related to a frequency, and the radiation intensity is expected to be at the thermal level as it is for electromagnetic electron-cyclotron emission (ECE) below the cutoff density. The emitting frequency of EBE compared with perpendicular ECE is Doppler shifted due to the nonvanishing N_{\parallel} component of the refractive index for the oblique angle of observation. In contrast to ECE, for nonresonant frequencies EBW radiation is not able to leave the plasma and is trapped inside the plasma as in a hohlraum (see the 70 GHz beam in Fig. 1). The origin of this radiation is nonlocal and we expect a thermal emission intensity of the average plasma temperature.

Experiments.—The experiments were performed at the W7-AS stellarator (major radius $R = 2.0$ m, minor radius

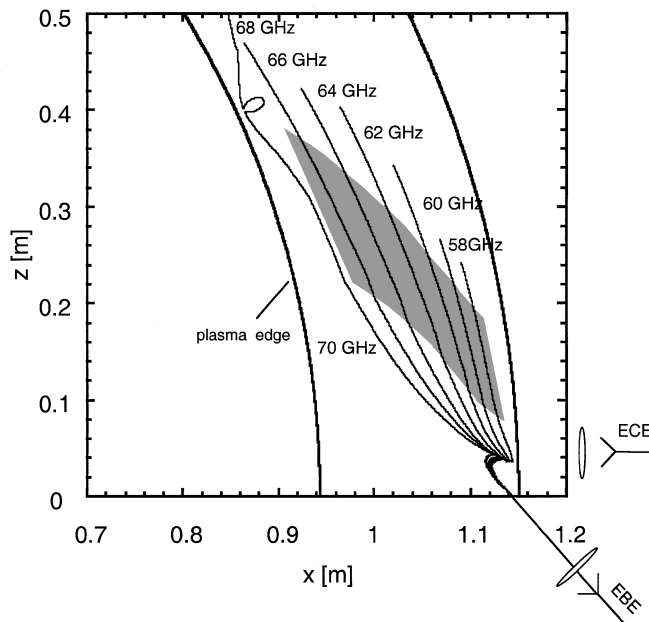


FIG. 1. Ray-tracing calculation of EBE at a central magnetic field of 2.1 T, a central temperature of 600 eV, and a central density of $0.9 \times 10^{20} \text{ m}^{-3}$. The rays are propagating in the equatorial plane.

$a = 0.18$ m). Since the standard ECE diagnostic at W7-AS uses fixed antennas with a viewing angle of 90° with respect to the magnetic field, the ECE radiometers were connected with an unused movable ECRH-launch antenna. A detailed description of W7-AS and its ECRH-launch system can be found in [4] and the ECE-radiometer-type is described in [5].

(1) *Calibration.*—The system was calibrated with thermal ECE (first harmonic O mode at $B_0 = 2.5$ T) at a perpendicular (90°) viewing angle and at plasma densities below the O -mode cutoff. It was taken into account that for oblique observation the O -mode radiation is elliptically polarized, whereas the receiving system is only sensitive to linearly polarized radiation.

(2) *Density threshold.*—The receiving mirror was turned to the optimum viewing angle of 47° with respect to the magnetic field and the plasma density was ramped up to above the cutoff density, as shown in Fig. 2. The plasma was sustained by two neutral beam injectors (NBI) with 360 kW power each. The central magnetic field was lowered to 2.1 T to compensate the Doppler shift of the EBE spectrum. For comparison, the plasma temperature measured with the soft-X-filter method for the central line of sight is plotted at the top of Fig. 2. Below, the low field side EBE radiation, the central EBE, and the high field side EBE are shown. When the central

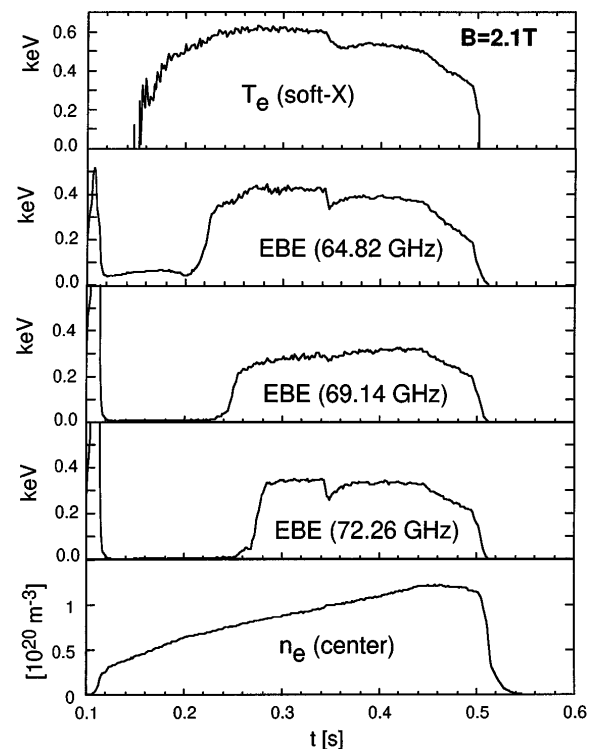


FIG. 2. Signals of an NBI sustained discharge with a density ramp. From the top: soft-X temperature, radiation temperature of the low field side edge EBE, central EBE, and high field side edge EBE, and central density. The temperature dip at 0.34 s is due to a perturbation induced by carbon laser blowoff.

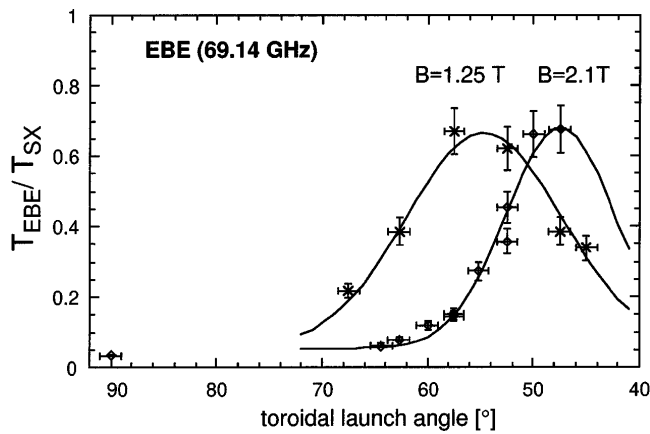


FIG. 3. Angular dependence of EBE for different central magnetic fields, for central density of $1 \times 10^{20} \text{ m}^{-3}$, and for a temperature of 600 eV. The signal is normalized to the central soft-X temperature.

density as measured with a microwave interferometer and by Thomson scattering reaches the cutoff density of the emitting frequency, the B - X - O window opens and EBE appears, as shown in Fig. 2.

(3) *Angular window.*—Scans of the viewing angle were performed for the first and second harmonic EBE as shown in Fig. 3 and the predicted angular windows at 47° for 2.1 T (69.14 GHz) and 55° for the second harmonic EBE at 1.25 T could experimentally be reproduced. The radiation temperature was up to 70% of the temperature measured by soft- X emission and Thomson scattering. This might be due to the reduced X - O conversion caused by density fluctuations at the cutoff surface as described in [2].

(4) *The EBE spectrum.*—First, ECE and EBE spectra are compared. The central magnetic field was set at 2.4 T for which both spectra are in the spectral range of our detection system (61–78 GHz). In Fig. 4 both the thermal ECE spectrum [first harmonic O mode, $n_e < n_{e,\text{cutoff}}$ (squares)] received by the ECRH antenna with 90° viewing angle and the EBE spectrum at 47° [first harmonic, $n_e > n_{e,\text{cutoff}}$ (circles)] of an NBI sustained plasma are shown. The ECE spectrum reflects the plasma temperature profile. The EBE spectrum is about 6 GHz Doppler shifted and shows the low field (frequency) side temperature gradient. The small pedestal at its low-frequency part may originate from stray radiation emitted at the low density plasma edge. In order to also record the high-frequency part of the spectrum, the magnetic field or the central electron-cyclotron resonance frequency was reduced by 0.4 T, corresponding to 11.2 GHz, respectively. As shown in Fig. 5, instead of a high field side decay, as is typical for ECE, the EBE spectrum has a slowly decreasing broadband high-frequency part. By a further shift of the EC resonance frequency, we found that the high-frequency part is emitted up to about 1.7 times the electron-cyclotron frequencies in the plasma. We think that this is the nonlocal “hohlraum”

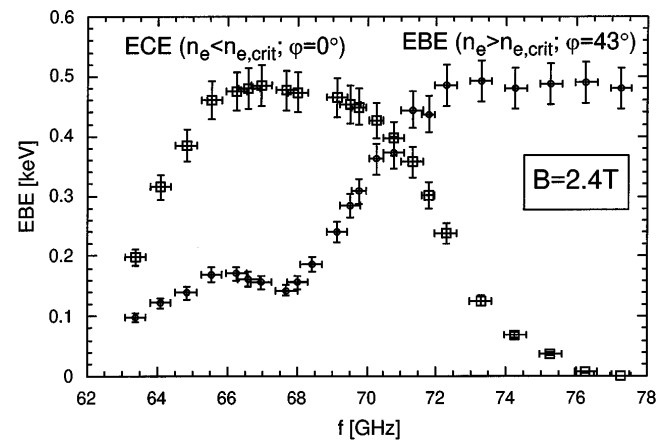


FIG. 4. Doppler-shifted EBE spectrum (circles) and ECE spectrum (squares) for similar discharges but at different densities. In the EBE discharge the central temperature was 700 eV.

radiation as has already been discussed in the previous section.

(5) *Cold pulses.*—These experiments were conducted to establish the relation between the frequency of the thermal EBE and the radial position of the emission zone. Temperature perturbations at the plasma edge were set by carbon laser blowoff. The amount of ablated carbon was matched to a value where we could find a sufficiently large temperature decrease in all EBE channels, but with a minimum disturbance of the plasma discharge, especially with no significant density increase. An example is shown in Fig. 2, where at 0.34 s the cold pulse was set. One could identify a steep temperature dip in the edge EBE channels (64.84 and 72.26 GHz), a small dip in the central channel (69.14 GHz), and nearly no change in the average plasma density. In Fig. 6 the amplitude and delay time, in

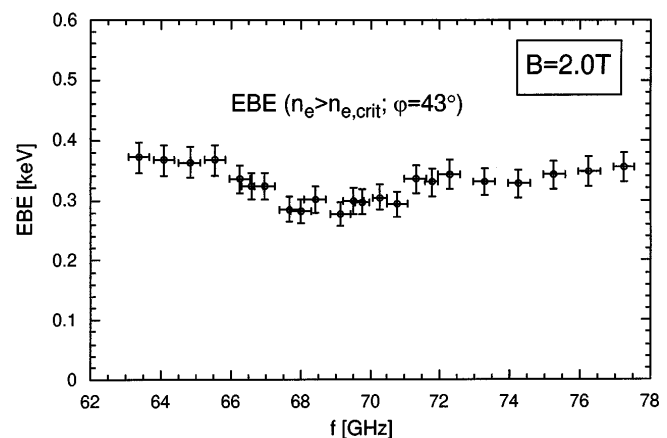


FIG. 5. High frequency part of the EBE spectrum. The central ECE resonance frequency is shifted by about 11.2 GHz in respect to Fig. 4. Because of the confinement degradation with decreasing magnetic field, the central temperature decreases to about 500 eV.

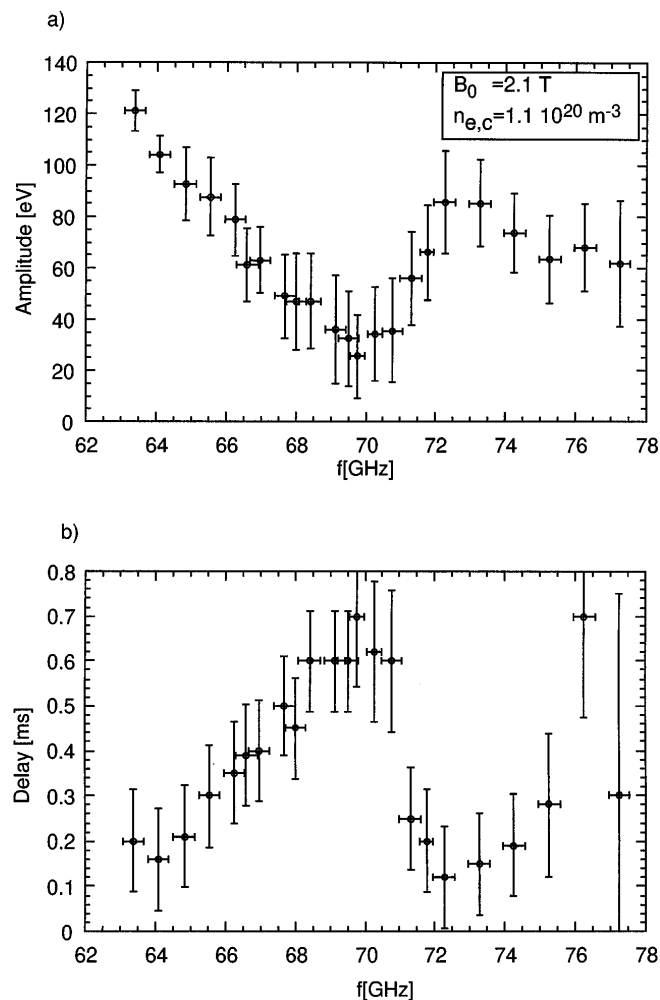


FIG. 6. (a) Amplitude decay and (b) delay time of the $1/e$ amplitude as a function of EBE frequency. This indicates the inward propagation of the temperature perturbation induced by carbon laser blowoff at the plasma edge, thus demonstrating the localization of the radiation origin.

which the signal reaches $1/e$ of the amplitude of the cold pulse, are plotted as a function of the emission frequency.

Assuming that the cold pulse propagates from the outer radii towards the center, both the amplitude and the delay time indicate that, for the thermal part of the spectrum, there is a clear relation between the emitted frequency and the radial position of the emission. For the spectrum above 73 GHz no amplitude variation and no clear phase attachment could be found, which indicates the nonlocal character of the high-frequency part of the EBE.

In summary, electron-cyclotron radiation from an over-dense plasma was detected with an oblique observation angle. This could be identified as electron Bernstein wave emission through the angular window of the inverse $O-X-B$ process ($B-X-O$). The emitted spectrum consists of two parts:

The thermal part reflects the local thermal emission of EBW and, in principle, a radial temperature can be reconstructed from this radiation.

The high-frequency part represents nonlocal hohlraum radiation since most of the EBW's are trapped inside the plasma, and only those rays which somehow obtain the optimal N_{\parallel} and N_{\perp} for the small angular window of the $B-X-O$ process can leave the plasma.

Both the local and nonlocal character of the EBE spectrum were demonstrated by cold wave propagation with laser blowoff.

Besides the renewed verification of the hot plasma wave theory and the insight into EBW physics in a fusion plasma, the EBE also opens a new operational window for electron-cyclotron diagnostics beyond the cutoff for fusion as well as for ionospheric research.

- [1] J. Preinhaelter and V. Kopecký, J. Plasma Phys. **10**, 1 (1973).
- [2] H.P. Laqua *et al.*, Phys. Rev. Lett. **78**, 18 (1997).
- [3] E. Mjølhus, J. Plasma Phys. **31**, 7 (1984).
- [4] H. Renner *et al.*, Plasma Phys. Control. Fusion **31**, 10 (1989).
- [5] H.J. Hartfuss *et al.*, Plasma Phys. Control. Fusion **39**, 1693 (1997).